Journal of Power Sources 222 (2013) 379–389

Contents lists available at SciVerse ScienceDirect

Journal of Power Sources

journal homepage: www.elsevier.com/locate/jpowsour

Model for investigation of oxygen transport limitation in a polymer electrolyte fuel cell

Takahisa Suzuki*, Kenji Kudo, Yu Morimoto

Toyota Central R&D Laboratories, Inc., Nagakute, Aichi 480-1192, Japan

HIGHLIGHTS

- ► Oxygen dissolution process from gas phase into the ionomer was included in the model.
- ► Dissolution kinetics were assessed using thin ionomer films on a Pt electrode.
- ► Agglomerate sizes were determined based on diffusion-limited currents.
- ► The estimated agglomerate size is close to that observed in the catalyst layer.
- ► Slow dissolution is the main hindrance to oxygen transport.

ARTICLE INFO

Article history:
Received 7 May 2012
Received in revised form
3 August 2012
Accepted 22 August 2012
Available online 10 September 2012

Keywords:
Polymer electrolyte fuel cell
Oxygen transport
Catalyst layer
Agglomerate size
Dissolution rate

ABSTRACT

A model for oxygen transport in the catalyst layer of polymer electrolyte fuel cells was developed. The model includes oxygen transport resistance for dissolution from the gas phase into the ionomer, which is typically assumed to be negligible in conventional models. The dissolution kinetics were experimentally assessed by measuring the diffusion-limited current density, i_d, in a planar Pt electrode covered with thin ionomer films as a function of film thickness. The extrapolation of i_d^{-1} to zero thickness reflects the dissolution resistance. The effect of dissolution resistance is added to a conventional agglomerate model of the catalyst layer as an additional cause of transport loss. The agglomerate size was determined so that the model predicted the same diffusion-limited current density as the experimental results. The agglomerate size was close to the particle size observed in scanning electron micrographs of the cross-section of the catalyst layer prepared by focused ion beam milling. In contrast, the conventional agglomerate model must adopt an agglomerate size that is larger by one order-of-magnitude than that experimentally observed. As a result, it is reasonable to attribute the hindrance of oxygen transport in the catalyst layer to the slow oxygen dissolution at the gas–ionomer interface, rather than to the presence of large agglomerates.

1. Introduction

The output voltage of a polymer electrolyte fuel cell (PEFC) is strongly affected by the mass-transport limitation of oxygen at high current densities, due to a decrease in the oxygen concentration at the catalyst surface. The oxygen concentration profile has been estimated using a multicomponent gas diffusion model [1] and Knudsen diffusion model [2], which reflect the transport of species in the pores of the electrodes. Agglomerate models [3,4], which will be reviewed and modified in this paper, have been employed to calculate the oxygen concentration in the ionomer that covers the catalyst. A clear understanding of where and how the concentration decreases and identification of the rate-determining process in the electrodes will facilitate the material development and component optimization of PEFCs.

Agglomerate models were introduced to predict current–voltage characteristics [3,4] on the basis of scanning electron microscopy (SEM), which indicated the agglomeration of Pt/C particles in the catalyst layer. The agglomerate model ascribes the increase in the Tafel slope with increasing current density to a decrease in the oxygen concentration near the center of the agglomerate. Mathematically, the agglomerate is simplified into a sphere (or a cylinder without pores) of a homogeneous mixture consisting of a carbon-supported catalyst and an ionomer. The agglomerate may be surrounded by a film of the ionomer. When the current density increases, the reaction preferably occurs near the surface of the agglomerate and most of the oxygen is consumed

* Corresponding author. Tel.: +81 561 71 7872; fax: +81 561 63 4120.
E-mail address: takahisa@mosk.tytlabs.co.jp (T. Suzuki).

0378-7753/$ – see front matter © 2012 Elsevier B.V. All rights reserved.
http://dx.doi.org/10.1016/j.jpowsour.2012.08.068

there. The model was validated by a comprehensive comparison between the model predictions and experimental results [5]. An agglomerate radius of between 0.1 and 1 μm was typically assigned in the previous studies [4–27].

If this model is sufficient to depict the catalyst layer, then the same size agglomerates should be observed in actual catalyst layers, and consequently, the agglomerates can be modified to improve the catalyst layer according to the model predictions. To our knowledge, no such study has been conducted and the agglomerate radius has been treated simply as a parameter that fits the model predictions to the experimental results.

This work proposes a model for the oxygen transport in the cathode catalyst layer. Cross-sections of catalyst layers with various ionomer loadings were observed to estimate the agglomerate size. The oxygen transport resistance of the ionomer was measured for thin films on an electrochemical cell and was separated into internal and external resistances. The latter is incorporated into the conventional agglomerate model as an additional cause of transport loss. The proposed model was assessed according to the current–voltage characteristics and the corresponding agglomerate size.

2. Experimental

2.1. Fabrication and characterization of membrane-electrode assemblies

Membrane-electrode assemblies (MEAs) with 13 cm^2 active areas were fabricated by hot pressing catalyst layer decals onto 25 μm thick Nafion membranes (NRE-211, DuPont). The anode (cathode) decals consisted of 10 wt% Pt/C (TEC10E10A, Tanaka Kikinzoku Kogyo) and a Nafion dispersion solution (DE2020 CS type, DuPont), and 30 wt% Pt/C (TEC10E30E, Tanaka Kikinzoku Kogyo) and DE2020 CS, respectively. Three cathode decals with different ionomer/carbon weight ratios (I/C) were applied. Platinum loading, I/C, thickness, and the porosity of the resulting anode and cathode catalyst layers are listed in Table 1. Developmental gas diffusion layers were inserted when the MEA was assembled into a cell fixture.

The cathode decals used for the MEAs in Table 1 were cut out and hot-pressed onto Nafion membrane for morphological observations. Cross-sections perpendicular to the membrane surface were prepared by focused ion beam (FIB; FB200A, Hitachi High-Technologies) milling. Cross-sections were observed using SEM (S-5500, Hitachi High-Technologies).

2.2. Measurement of the oxygen transport properties of thin ionomer films

The oxygen transport characteristics were measured using thin ionomer films prepared on an electrochemical cell (011598, BAS), as shown in Fig. 1(a) and (b), in which Pt film electrodes were printed on a quartz plate. Three out of eight electrodes were platinized and used for the measurement. Electrodes A (1 mm × 2.5 mm), B (10 μm × 2.5 mm), and C (10 μm × 2.5 mm) served as the counter, working, and pseudo-reference electrodes, respectively. The gap between the working and pseudo-reference electrodes was 30 μm. With 0.1% oxygen, the quasi-steady-state diffusion-controlled current density of the working electrode would be approximately 1 A cm^{-2} between 1 and 1000 s using the value of gas diffusivity [28]. Nafion films were spin-coated on the electrodes, as shown in

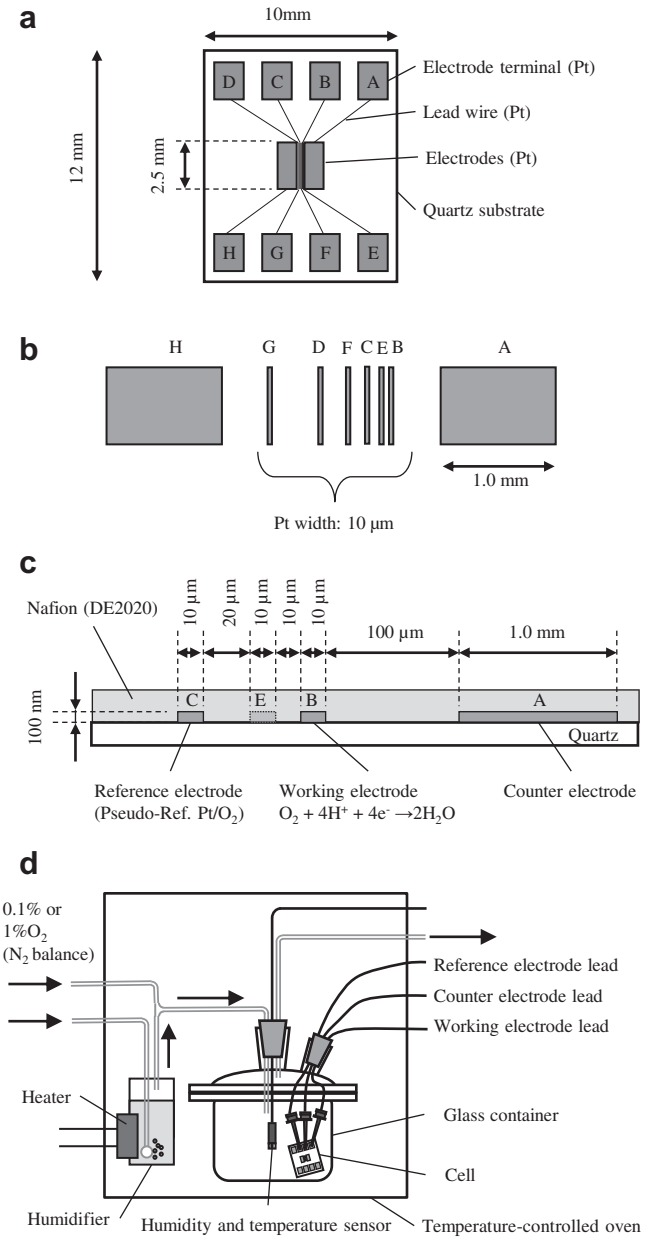

Fig. 1. Schematic illustration of the cell used to measure oxygen transport properties of an ionomer film. (a) Top view of the cell, (b) enlarged view of the electrodes, (c) side view around the working electrode B, and (d) experimental setup.

Table 1
Parameters of MEAs.

MEA	Anode				Cathode					
	Pt loading (mg cm^{-2})	I/C	Thickness (μm)	Porosity (%)	Pt loading (mg cm^{-2})	I/C	Thickness (μm)	Porosity (%)	Ionomer volume fraction (%)	ECSA (cm^2_{Pt} cm^{-2})
a	0.025	1.0	8	71	0.094	0.5	5	66	11	42
b	0.025	1.0	8	71	0.094	0.75	5	60	17	40
c	0.023	1.0	8	74	0.109	1.0	6	56	22	49

Fig. 1(c), at room temperature using Nafion dispersion solution (DE2020, DuPont) diluted with 1-propanol. Unwanted film in the peripheral area was rubbed off with a polyethylene foam swab dampened with ethanol. The film was further dried in air at 130 °C for 1 h. Fig. 1(d) shows the experimental setup used for the measurement. The cell was enclosed in a glass container with a nominal capacity of 200 mL and placed in a temperature-controlled oven. Oxygen was diluted with nitrogen to 1% (for films thicker than 400 nm) or 0.1% (for films thinner than 400 nm) and supplied to the cell at 100 mL min^{-1}. The relative humidity of the gas was controlled by mixing fully humidified gas and dry gas. Cyclic voltammetry (CV) was performed at 5 mV s^{-1} between the potential just above hydrogen evolution and 100 mV vs. the pseudo-reference electrode using an electrochemical measurement system (HZ-5000/HAG1512m, Hokuto Denko). The thickness of the films was measured using a stylus profiler (Dektak 3 Surface Profiler, Veeco) after the electrochemical measurement.

For comparison, the solubility and diffusion coefficient of oxygen were measured for a 96 μm thick cast Nafion film using a microelectrode cell. Fig. 2(a) shows a schematic of the experimental setup. In this cell, the Nafion film is sandwiched between a 50 μm diameter Pt microelectrode and a polytetrafluoroethylene (PTFE) filter through which oxygen is supplied. The edge of the film is attached to NRE-211 Nafion membrane with counter (platinized Pt) and reference electrodes (RHE) attached, as shown in Fig. 2(b). The solubility and diffusion coefficient were determined from chronoamperometric measurements with a potential step applied from 1.1 to 0.4 V vs. RHE [29]. The measurement was conducted at 80 °C under three different relative humidity (RH) conditions.

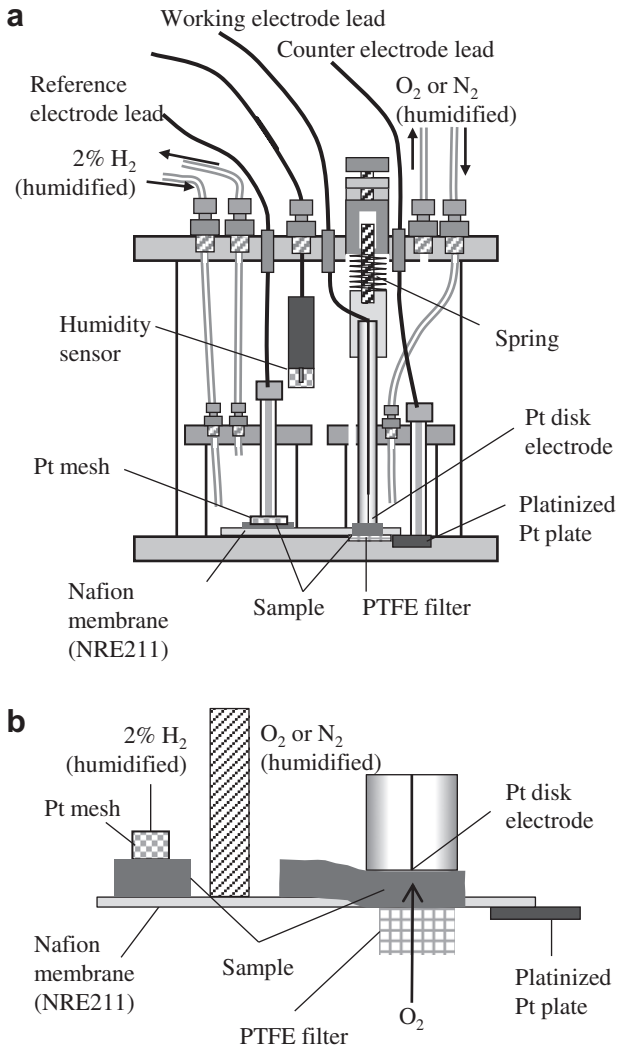

Fig. 2. Schematic illustration of the cell used to measure oxygen transport properties of a 96 μm thick film.

2.3. Measurement of the MEA performance

Electrochemical measurements of the MEAs were conducted using a charge/discharge unit (5 V, 30 A, Hokuto Denko) with a fuel cell testing system (Chino). The reactant gas (hydrogen or oxygen) and nitrogen were mixed and humidified by bubbling through water at controlled temperatures. The flow rates of the anode and cathode dry gases were always set at 500 and 2000 standard cubic centimeter per minute (SCCM), respectively, to ensure reproducibility of the RH and a sufficiently high stoichiometric ratio. A high stoichiometric ratio helps to justify the omission of the in-plane variation in the mathematical model described later. The partial pressures of the gases at the inlet can be calculated from the flow rates of the gases, the water vapor pressure, and the total pressure.

The current–voltage characteristics of the MEA and the electrochemical surface area (ECSA) of the cathode were measured at 80 °C and 140 kPa. Firstly, hydrogen–nitrogen and oxygen–nitrogen mixtures with 70% RH were supplied to the anode and cathode, respectively. The RH was selected to ensure that the cell was free from flooding over the entire range of the measured current density. The partial pressure of hydrogen was set at 93 kPa, and that of oxygen was set at 1.9, 9.3, or 19.5 kPa. The current–voltage characteristics were measured by sweeping the current density at 7.7 mA cm^{-2} s^{-1} from open-circuit voltage to 0.1 V for each oxygen partial pressure. Resistance was simultaneously measured at 500 Hz. CV was conducted between 0.05 and 1.2 V at 0.1 V s^{-1} with hydrogen and nitrogen at 100% RH supplied to the electrodes.

3. Mathematical model

3.1. Oxygen transport model

Fig. 3 illustrates the oxygen concentration profile across an ionomer film on a planar electrode where the oxygen reduction reaction (*ORR*) occurs. When the diffusion-limited current density, i_d, is observed, the oxygen flux, J_d, can be described by Fick's law of diffusion with constant oxygen diffusivity:

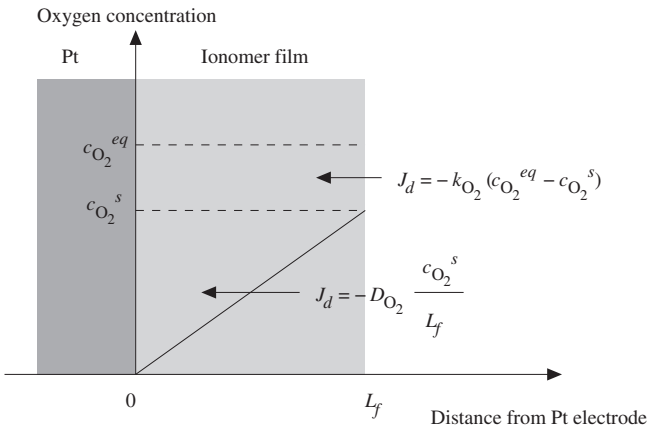

Fig. 3. Oxygen concentration profile for an ionomer film on a planar Pt electrode when a diffusion-limited current is observed.

$$-\frac{i_d}{n_{ORR}F} = J_d = -D_{O_2}\frac{c^s_{O_2}}{L_f}, \tag{1}$$

where n_{ORR} is the number of electrons transferred per oxygen molecule in the *ORR*, F is Faraday's constant, D_{O_2} is the oxygen diffusion coefficient of the ionomer, $c^s_{O_2}$ is the oxygen concentration in the ionomer at the gas–ionomer interface, and L_f is the film thickness. The process of oxygen dissolution from the gas phase to the ionomer film is modeled as surface reactions that are dependent on the concentrations of oxygen in both phases [30]:

$$J_d = -k_{O_2}\left(c^{eq}_{O_2} - c^s_{O_2}\right), \tag{2}$$

where k_{O_2} is a rate constant and $c^{eq}_{O_2}$ is the equilibrium concentration of oxygen in the ionomer, which is a function of the partial pressure of oxygen. From Eqs. (1) and (2),

$$\frac{1}{i_d} = \frac{1}{n_{ORR}Fc^{eq}_{O_2}D_{O_2}}L_f + \frac{1}{n_{ORR}Fc^{eq}_{O_2}k_{O_2}}. \tag{3}$$

Therefore, the dissolution rate constant, k_{O_2}, can be determined if the diffusion-limited current density obeys Eq. (3) for various film thicknesses. An additional term that is independent of film thickness appears if there is some type of concentration jump at the ionomer–electrode interface. The interfacial resistance to oxygen transport from ionomer–electrode and gas–ionomer interfaces cannot be distinguished from experiments with a planar electrode. For simplicity, we assume that the resistance exists only at the gas–ionomer interface.

3.2. Performance model overview

The performance model presented here describes steady-state species transport between two gas diffusion layer (GDL) surfaces of an MEA at constant temperature. The MEA is modeled as a set of layers containing an electrolyte membrane, two catalyst layers, two microporous layers (MPLs), and two GDLs. The phenomena described are (a) the transport of gas species (hydrogen, oxygen, water vapor, and nitrogen) through the pores in the catalyst layers, MPLs, and GDLs, (b) dissolution of oxygen from the gas phase to the ionomer in the cathode catalyst layer, (c) exchange of water between the ionomer and pores in the catalyst layers, (d) oxygen transport through the ionomer in the cathode catalyst layer, (e) water and proton transport through the electrolyte membrane and the ionomer in the catalyst layers, (f) hydrogen oxidation reaction (*HOR*) in the anode catalyst layer, and (g) *ORR* in the agglomerates of the cathode catalyst layer. Species conservation equations in the through-plane direction are solved under given boundary conditions at the GDL surfaces and are implemented using gPROMS ModelBuilder (Process Systems Enterprise).

3.3. Conservation law

The general expression of the conservation law for a steady state can be described as:

$$\frac{\partial N_i}{\partial x} = \Phi_i, \tag{4}$$

where N_i is the flux of species i, x is the through-plane position, and Φ_i is the volumetric rate of production of species i. The expression for N_i varies depending on species i. The rate Φ_i is negative when species i is consumed.

The flux of gas species through the pores is the sum of convective flux and the diffusive flux:

$$N_i = CX_i v + J_i, \tag{5}$$

where C is the concentration of the gas, X_i is the mole fraction of species i, v is the velocity, and J_i is the diffusive flux of species i. The diffusive flux is described by the Stefan–Maxwell equation:

$$\frac{\partial X_i}{\partial x} = -\sum_{\substack{j=1\\ j\neq i}}^{M}\frac{X_jJ_i - X_iJ_j}{C\widehat{D}^{eff}_{ij}}, \tag{6}$$

where $\widehat{D}^{eff}_{ij}$ is the effective binary diffusion coefficient of species i–j system in the given layer and M is the number of gas species.

The water flux through the ionomer is the sum of diffusive flux and electroosmotic flux:

$$N_{H_2O} = -\frac{\rho_I}{m_I}D^{eff}_{H_2O}\frac{\partial\lambda}{\partial x} + \frac{\beta}{F}i, \tag{7}$$

where N_{H_2O} is the water flux, ρ_I is the dry density of the ionomer, m_I is the equivalent weight (EW) of the ionomer, $D^{eff}_{H_2O}$ is the effective diffusion coefficient of water in the given layer, λ is the water content of the ionomer, β is the number of water molecules accompanying a proton, and i is the proton current density.

The proton current density is described by Ohm's law:

$$i = -\kappa^{eff}\frac{\partial\phi}{\partial x}, \tag{8}$$

where κ^{eff} is the effective proton conductivity of the ionomer in the given layer, and ϕ is the electrolyte potential. Liu et al. [31] observed that the ionomer captured within the small pores of primary carbon particles does not contribute to the proton conductivity across the electrode; therefore, two models were compared for the effective proton conductivity in the cathode catalyst layer. One model, which will be referred to as the film conduction (FC) model, assumes that only the ionomer film that covers the agglomerate contributes to the effective proton conductivity:

$$\kappa^{eff} = {\varepsilon_{I,f}}^{1.5}\kappa, \tag{9}$$

where $\varepsilon_{I,f}$ is the volume fraction of the ionomer film in the catalyst layer and κ is the proton conductivity of the ionomer. The other model, which will be referred to as the bulk conduction (BC) model, assumes that all the ionomer in the catalyst layer contributes to the proton conductivity:

$$\kappa^{eff} = \varepsilon_I^{1.5}\kappa, \tag{10}$$

where ε_I is the volume fraction of the ionomer in the catalyst layer. Bruggeman's approximation [32] is used in both models. The BC model is applied for the anode catalyst layer.

The *HOR* rate is described as a linearized form of the Butler–Volmer equation. The exchange current density is assumed to have linear dependence on the hydrogen concentration. Hence, the volumetric rate of hydrogen production in the pores of the anode catalyst layer Φ_{H_2}, is

$$\Phi_{H_2} = -\frac{s_a}{n_{HOR}F}i^{ref}_{HOR}\frac{c_{H_2}}{c^{ref}_{H_2}}\frac{2F}{R_uT}\eta, \tag{11}$$

where s_a is the catalyst surface area per unit volume of the anode catalyst layer, n_{HOR} is the number of electrons transferred per hydrogen molecule during the *HOR*, i^{ref}_{HOR} is the reference current density, c_{H_2} is the hydrogen concentration in the ionomer, $c^{ref}_{H_2}$ is the

reference hydrogen concentration, R_u is the universal gas constant, T is the temperature, and η is the overpotential.

The volumetric production rate of water vapor in the pores of the catalyst layer Φ_{H_2O}, is proportional to the difference between the water activity that corresponds to the water content of the ionomer a_λ, and the water activity in the pore, a_g:

$$\Phi_{H_2O} = s_v k_{H_2O} \frac{p_{sat}}{R_u T}(a_\lambda - a_g), \tag{12}$$

where s_v is the area of the interface between the ionomer and the gas phase, k_{H_2O} is the evaporation rate constant, and p_{sat} is the saturation water vapor pressure at temperature T.

3.4. Agglomerate model

The flooded agglomerate model, in which the Pt/C agglomerate is filled with an ionomer, is applied to calculate the volumetric rate of oxygen production in the cathode catalyst layer, Φ_{O_2}. The catalyst layer is comprised of n spherical particles per unit volume of the catalyst layer, which yields its porosity, ε_0. The particle is comprised of an agglomerate of radius R covered with an ionomer film of thickness δ. Hence, n is given by:

$$1 - \varepsilon_0 = \frac{4}{3}\pi(R+\delta)^3 n. \tag{13}$$

The area s_v is therefore calculated as:

$$s_v = 4\pi(R+\delta)^2 n. \tag{14}$$

Oxygen transported through the pores in the catalyst layer dissolves into the ionomer, diffuses through the ionomer film and into the agglomerate where it reacts. The species conservation in an agglomerate particle covered with an ionomer film is described as follows. The radial flux of oxygen in the ionomer is assumed to obey Fick's law of diffusion:

$$J_{O_2} = \begin{cases} -D_{O_2}^{eff}\dfrac{dc_{O_2}}{dr}, & 0 \le r \le R \\ -D_{O_2}\dfrac{dc_{O_2}}{dr}, & R \le r < R+\delta \end{cases}, \tag{15}$$

where J_{O_2} is the oxygen flux in the radial direction, c_{O_2} is the oxygen concentration in the ionomer, $D_{O_2}^{eff}$ is the effective oxygen diffusivity in the agglomerate, and D_{O_2} is the oxygen diffusivity in the ionomer film. The conservation equations for oxygen are:

$$-D_{O_2}^{eff}\frac{d^2c_{O_2}}{dr^2} - D_{O_2}^{eff}\frac{2}{r}\frac{dc_{O_2}}{dr} = -\frac{1}{n_{ORR}F}s_{agg}i_{ORR}^{ref}\frac{c_{O_2}}{c_{O_2}^{ref}}\exp\left(-\frac{\alpha F}{R_u T}\eta\right), \quad 0 \le r \le R \tag{16}$$

$$-D_{O_2}\frac{d^2c_{O_2}}{dr^2} - D_{O_2}\frac{2}{r}\frac{dc_{O_2}}{dr} = 0, \quad R \le r \le R+\delta, \tag{17}$$

where s_{agg} is the catalyst area per unit volume of the agglomerate, i_{ORR}^{ref} is the reference current density, $c_{O_2}^{ref}$ is the reference oxygen concentration, and α is the apparent transfer coefficient. Although the solution of Eq. (16) can be derived analytically, we decided to solve this equation numerically for reasons of robustness.

The production rate of oxygen in an agglomerate Φ_1, is given by:

$$\Phi_1 = 4\pi R^2 J|_{r=R} = -4\pi R^2 D_{O_2}^{eff}\left.\frac{dc_{O_2}}{dr}\right|_{r=R}. \tag{18}$$

The volumetric rate of oxygen production in the catalyst layer is related to that in an agglomerate by:

$$\Phi_{O_2} = n\Phi_1 \tag{19}$$

The oxygen concentration in the ionomer film at the gas–ionomer interface is treated according to Eq. (2). The steady-state flux through the interface can be given as:

$$J_{O_2} = -k_{O_2}\left(c_{O_2}^{eq} - c_{O_2}^{R+\delta}\right), \tag{20}$$

where J_{O_2} is the flux from the ionomer to the gas phase and $c_{O_2}^{R+\delta}$ is the oxygen concentration in the ionomer at the interface. The concentration $c_{O_2}^{eq}$ is calculated from Henry's law. If the gas–ionomer interface is always in equilibrium, then

$$c_{O_2}^{R+\delta} = c_{O_2}^{eq} \tag{21}$$

is used instead of Eq. (20). Eq. (21) is equivalent to the assumption made by Jaouen et al., that the oxygen concentration at the surface of the agglomerate is always proportional to its concentration in the gas phase [4].

For consistency, the composition of the cathode catalyst layer should satisfy:

$$\sigma = (1-\varepsilon_0)\left(1 - \varepsilon_{I,agg} - \frac{1}{y}\frac{\rho_I}{\rho_{CB}}\left\{\varepsilon_{I,agg} + \left[\left(1+\frac{\delta}{R}\right)^3 - 1\right]\right\}\right) \frac{1}{\left(1+\frac{\delta}{R}\right)^3} L_{CL}\rho_{Pt}, \tag{22}$$

where σ is the catalyst loading, $\varepsilon_{I,agg}$ is the volume fraction of the ionomer in the agglomerate, y is I/C, ρ_I, ρ_{CB}, and ρ_{Pt} are the true density of the ionomer, support (carbon black), and catalyst (Pt), respectively, and L_{CL} is the thickness of the catalyst layer. In Eq. (22), the ionomer volume fraction $\varepsilon_{I,agg}$ and ratio δ/R are left undetermined.

3.5. Parameters for performance calculation

The following parameters were used to calculate the current–voltage characteristics. The values given in Table 1 were used as the structural parameters of the catalyst layers. The ECSAs deduced from CV were used for the cathode catalyst layers (Table 1). Other structural/physical parameters that are commonly used are listed in Table 2. Thickness, porosity, Pt area, and ionomer parameters approximate to the actual parameters for the MEAs. The rate

Table 2
Common structural/physical parameters.

Parameter	Value
Thickness of GDL substrate	2×10^{-4} m
Porosity of GDL substrate	0.8
Anode MPL thickness	6.6×10^{-5} m
Cathode MPL thickness	6×10^{-5} m
Porosity of MPL	0.5
Membrane thickness	2.5×10^{-5} m
Dry density of ionomer	1980 kg m^{-3}
EW of ionomer	1100 g equiv^{-1}
Anode Pt area per unit volume	1.25×10^6 m$^2_{Pt}$ m^{-3}
Reference current density for *HOR*	5×10^3 A m$^{-2}_{Pt}$
Reference concentration for *HOR*	23.916 mol m^{-3}
Reference current density for *ORR*	5×10^{-3} A m$^{-2}_{Pt}$
Reference concentration for *ORR*	3.041 mol m^{-3}
Apparent transfer coefficient for *ORR*	1
Rate constant of water evaporation	100 m s^{-1}

constant of water was selected to be sufficiently large so that the ionomer is almost at equilibrium with water vapor in the pore. The material properties are summarized in Appendix A. The operating conditions corresponded to those used for the experiment.

In this work, two models for the oxygen transport at the gas–ionomer interface were compared. The interface nonequilibruim (IN) model uses Eq. (20), where the concentration decreases with increasing oxygen flux into the ionomer. The interface equilibrium (IE) model uses Eq. (21) instead of Eq. (20), where the oxygen concentration in the ionomer at the interface is always at the equilibrium value.

4. Results and discussion

4.1. Characterization of the catalyst layer

Fig. 4 shows secondary electron images of the FIB cross-section of the cathode catalyst layer with different I/C, in addition to the Pt/C (TEC10E30E) material (Fig. 4(b)). Fig. 4(a) shows homogeneous structures on a scale of ca. 1 μm. This homogeneity justifies using the volume fraction of the components that do not vary with the through-plane position in the model. The Pt/C particle sizes shown in Fig. 4(b) range from 10 to 50 nm or more. Fig. 4(c), (e), and (g) shows that the catalyst layer comprises interconnecting particles

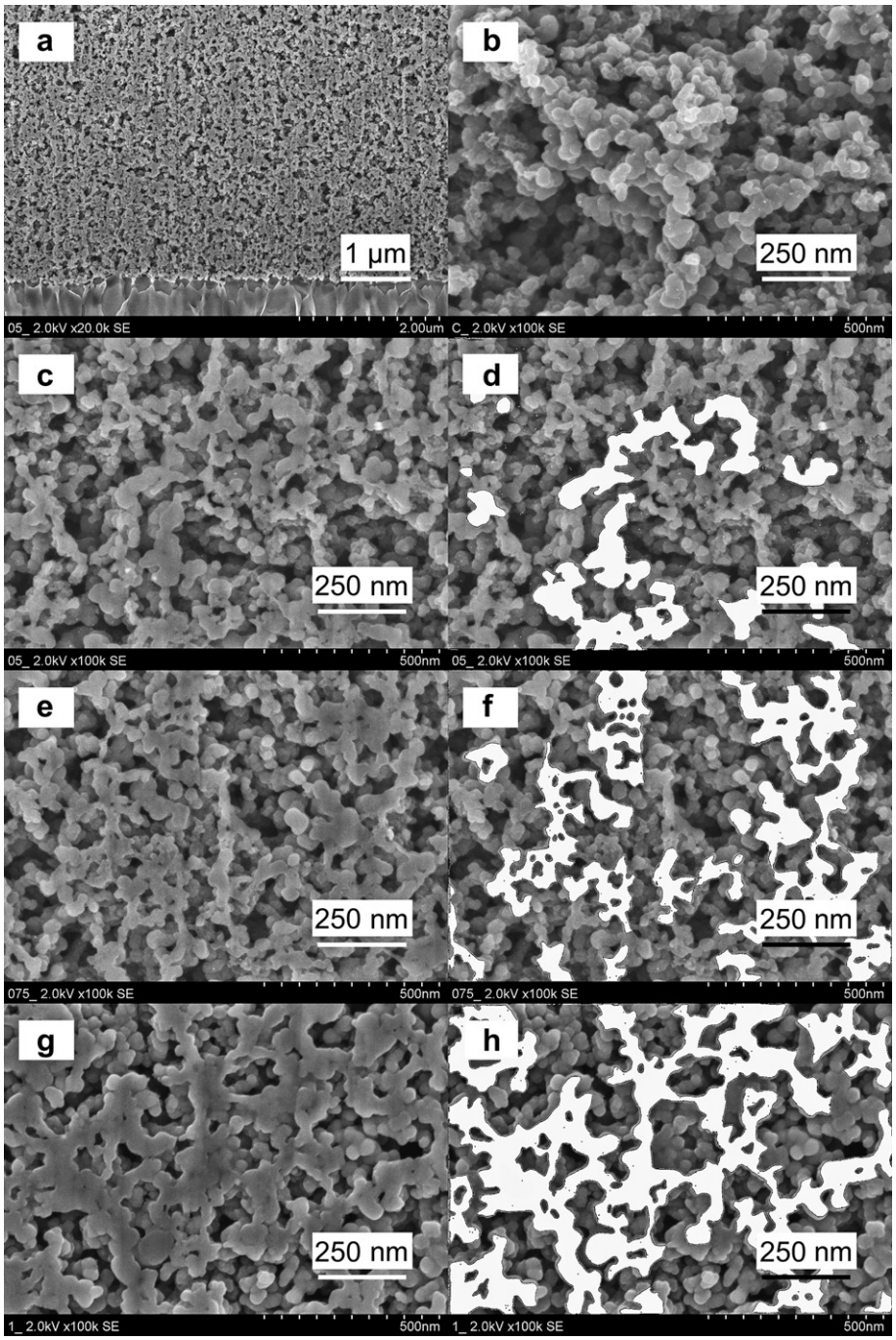

Fig. 4. Secondary electron images for (a) FIB cross-section of a cathode catalyst layer with I/C = 0.5 at 20,000× magnification, (b) Pt/C particles at 100,000× magnification, and (c–h) FIB cross-sections of the cathode catalyst layer at 100,000× magnification. (c,d) I/C = 0.5; (e,f) I/C = 0.75; (g,h) I/C = 1.0. Cross-sections are highlighted in (d), (f), and (h).

with diameters from 10 to 50 nm, which is close to that for the Pt/C particles. These three images also show that voids near the contact point between particles become filled as I/C increases.

Fig. 4(d), (f), and (h) highlights the cross-section of the catalyst layer and reveal that there are no large (200–2000 nm) ionomer-filled spheres that correspond to the agglomerate assumed in the previous models. Instead, the Pt/C particles adhere together to create the framework of the catalyst layer and the ionomer fills the voids between the particles. Although no large agglomerates were observed in the micrographs, relatively tightly-packed and loosely-packed regions were evident, especially for large I/C. If the tightly-packed region is regarded as an agglomerate, then the size appears to range from approximately 50–100 nm. Although the size is close to that of primary Pt/C particles, we assume that the agglomerate model is still applicable to the experimental catalyst layers, because a significant amount of Pt is supported inside this type of carbon support and on its surface [33] and the Pt utilization is more than 90% at 80 °C with>60% RH [34].

4.2. Oxygen transport properties

Fig. 5 shows representative cyclic voltammograms of Pt covered with thin Nafion films of different thicknesses under a diluted oxygen atmosphere. The reduction current of O_2 is observed below 0 V vs. the pseudo-reference electrode. As the potential decreases, the reduction current density initially increases, followed by an apparent plateau, and then increases abruptly with hydrogen evolution. The reduction current in the intermediate potential region increases with decreasing film thickness. The concentration

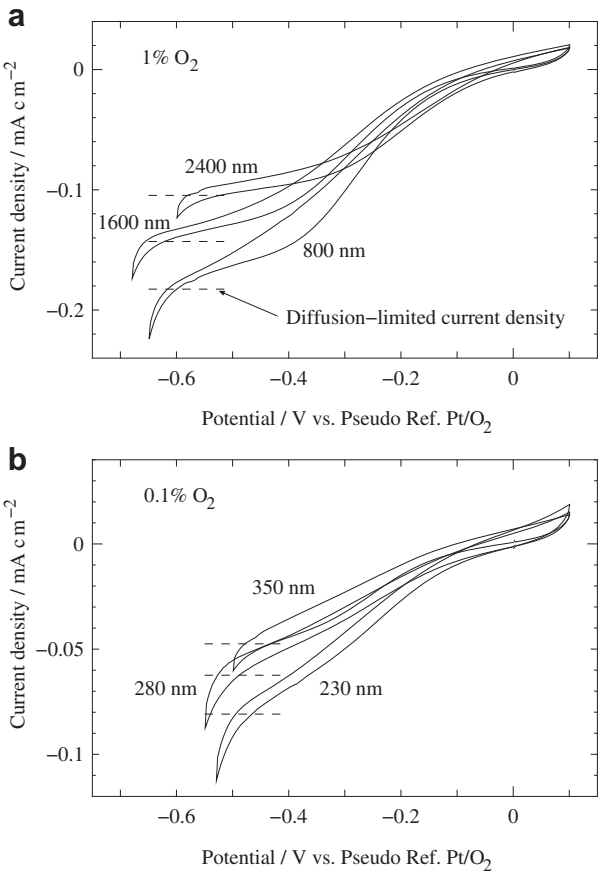

Fig. 5. Cyclic voltammograms of a Pt film electrode covered with thin Nafion films of various thickness under (a) 1% and (b) 0.1% O_2 at 80 °C and 60% RH.

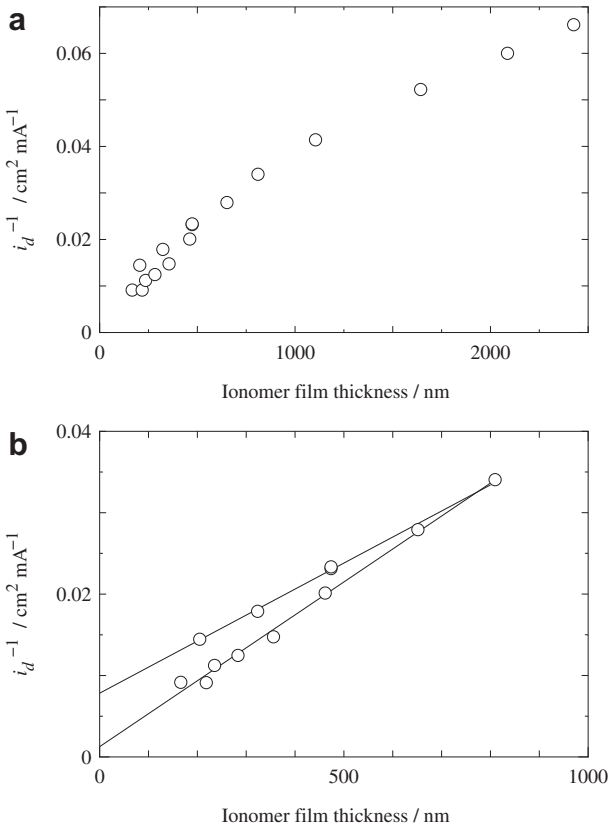

Fig. 6. (a) Relationship between the reciprocal of i_d and the ionomer film thickness at 80 °C and 60% RH, and (b) an enlarged view of (a) with lines added to indicate the range of the *y*-intercept.

drop in the gas phase is negligible, because the measured current density is sufficiently smaller than the diffusion-controlled current density calculated from the gas diffusivity. Although no clear current plateau was observed in the intermediate potential region, especially for thinner films, it was assumed that the reaction was almost under mass-transport control; therefore, the intersection of linear extrapolation lines from the apparent current plateau and the hydrogen evolution current was taken as the diffusion-limited current, as indicated by the dashed lines in Fig. 5. While true diffusion-limited currents can be larger than that estimated, we assume that the error is not significantly large.

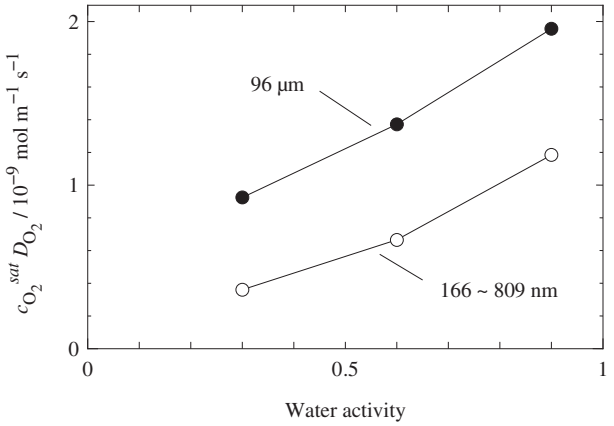

Fig. 7. Oxygen permeability of ionomer films at 80 °C as a function of water activity. (○): films with thicknesses between 166 and 809 nm; (●): 96 μm thick film.

Table 3
Oxygen permeability values.

Source	$c_{O_2}^{sat} D_{O_2}$ / 10^{-9} mol m^{-1} s^{-1}	T/K	a	Ionomer
This work	0.924[a]	353	0.3	Cast Nafion
This work	1.37[a]	353	0.6	Cast Nafion
This work	1.96[a]	353	0.9	Cast Nafion
Sethuraman et al. [35]	1.817	353	1	Nafion 117
Sethuraman et al. [35]	2.695	348	1	Nafion 112
Parthasarathy et al. [36]	0.77[a]	353	1	Nafion 117

[a] Oxygen solubility is converted to the value at 1 atm by dividing the measured solubility by the oxygen pressure.

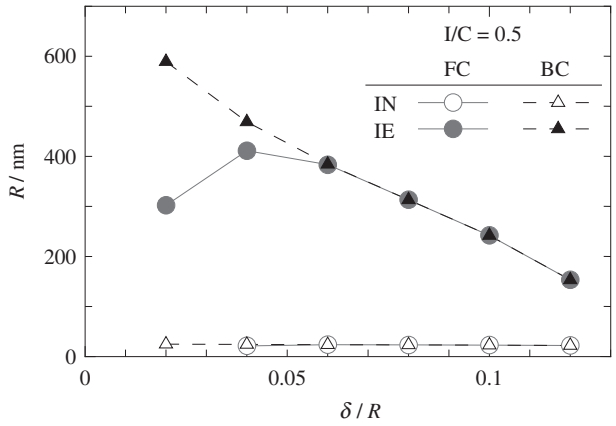

Fig. 8. Calculated agglomerate radius R, for the different models with I/C = 0.5.

The observed diffusion-limited current density was divided by the partial pressure of oxygen to eliminate the effect of the partial pressure difference. The inverse of the resulting current density, i_d^{-1}, increases with increasing film thickness, as shown in Fig. 6(a). The slope above 1000 nm is smaller than that below 1000 nm. Above 1000 nm, hemicylindrical diffusion through the ionomer film can be considered comparable to the linear diffusion normal to the electrode, of which the width is 10 μm. Below 1000 nm, the hemicylindrical diffusion becomes insignificant and linear diffusion through the film is dominant. Fig. 6(b) shows more detailed results below 1000 nm, where although the data are somewhat dispersed, i_d appears to obey Eq. (3).

The permeability, $c_{O_2}^{eq} D_{O_2}$, was obtained from the slope of the regression line by fitting the data, and the results are shown in Fig. 7 as a function of water activity. The permeability of the 96 μm thick film is also shown and is compared with the values in the literature in Table 3. The permeability obtained at a water activity of 0.9 is between those reported by Sethuraman et al. [35] for Nafion 112 and Nafion 117 at a water activity of 1, but larger than that reported by Parthasarathy et al. [36]. The dependence of permeability on the water activity is similar to that reported by Takamura et al. [37]. It should be noted that the thin films (<809 nm thick) have lower permeabilities than thick films. A similar trend was reported by Siroma et al. [38], where the proton conductivity decreased with decreasing film thickness; the authors pointed out the possibility that thin films absorb less water than thick films. If the water content of thin films is less than that of thick films, it is reasonable that oxygen permeability, which decreases with decreasing water content [39], is also depressed in thin films. We therefore assumed in the model that the water content of the ionomer in the cathode catalyst layer is half that of thick membranes at the same water activity.

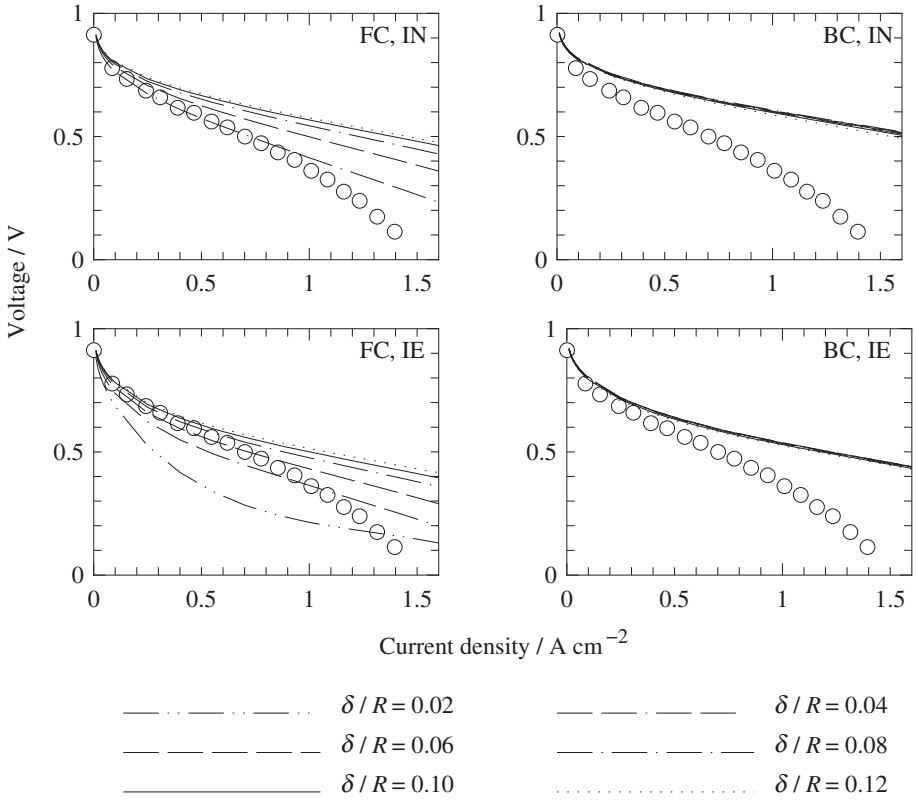

Fig. 9. Calculated performance curves with I/C = 0.5 for four different models and δ/R parameters. Experimental data are indicated by circles for comparison.

The product $c_{O_2}^{eq} k_{O_2}$ was obtained from the y-intercept of the same regression line and ranged from 3.2×10^{-3} to 2.0×10^{-2} mol m^{-2} s^{-1} at 60% RH. The nonzero value of the intercept implies that the oxygen dissolution process causes transport loss in the cathode catalyst layers, where much thinner ionomer films cover the Pt particles. A comparison of the first and second terms on the right-hand side of Eq. (3) shows that the dissolution process becomes more significant than the diffusion process when the film thickness L_f, becomes less than D_{O_2}/k_{O_2}, which is 100 nm ($= c_{O_2}^{eq} D_{O_2}/c_{O_2}^{eq} k_{O_2} \sim (1 \times 10^{-9}$ mol m^{-1} s$^{-1})/(1 \times 10^{-2}$ mol m^{-2} s^{-1})) from the order-of-magnitude estimate. The thickness of the ionomer covering is less than 100 nm, as shown in Fig. 4; therefore, the dissolution process should have a significant effect on the performance of the catalyst layers. The resistance to oxygen dissolution, $(c_{O_2}^{eq} k_{O_2})^{-1}$, was more than three times larger than that to oxygen diffusion, $L_f (c_{O_2}^{eq} D_{O_2})^{-1}$, with a typical film thickness in the catalyst layer, $L_f = 10$ nm.

4.3. Agglomerate size and MEA performance

The agglomerate size cannot be estimated from the SEM micrographs of the FIB cross-section, because the section does not always pass through the center of the particles. Therefore, the particle size determined from the micrographs was only used for comparison as an alternative method to determine the agglomerate size. The possible range of δ/R can be determined from the condition of $\varepsilon_{I,agg} > 0$. For each δ/R, the agglomerate radius R can be determined so that the model prediction and the experimental value are the same at one point on the performance curve. The current density at ca. 0.1 V when the oxygen partial pressure is at 1.9 kPa was selected. Under this condition, the current density can be regarded as the diffusion-limited current density. Fig. 8 shows the agglomerate radius as a function of δ/R with the smallest dissolution rate, $c_{O_2}^{eq} k_{O_2} = 3.2 \times 10^{-3}$ mol m^{-2} s^{-1}. The IE model gives a larger R than the IN model. The difference between the proton conduction models does not affect R, except for low δ/R, where the FC model gives larger ohmic loss than the BC model. The value of δ/R was determined so that the model prediction was close to the performance curve when the cell was operated at an oxygen partial pressure of 19.5 kPa. Fig. 9 shows a comparison of the predicted performance curves for various δ/R with the experimental data. No model prediction fits the performance curve over the entire range of current density, but the models and δ/R parameter can be selected to fit at current densities less than 0.5 A cm^{-2}. The change in δ/R produces a small change in the performance curve for the BC model. In contrast, the voltage in the FC model varies within the current density range, because the effective conductivity at the catalyst layer decreases with decreasing δ/R. No appropriate parameter could be found for the BC model with I/C = 0.5. Therefore, focus was made on the results of the FC model, and the values of R and δ are listed in Table 4. For the IN model, the sizes of the ionomer film-covered agglomerates were from 44 to 81 nm, which is similar to the particle size shown in the micrographs of Fig. 4. The increase in particle size with I/C corresponds to the filling of voids between Pt/C particles. In contrast, for the IE model, the agglomerate particle size is more than 400 nm and probably ca. 700 nm. However, agglomerates of that large size were not evident from SEM observation.

Table 4
Comparison of agglomerate radius R, ionomer film thickness δ, and the particle size, $2(R + \delta)$.

MEA	Cathode I/C	Model							
		IN				IE			
		δ/R	R/nm	δ/nm	$2(R+\delta)$/nm	δ/R	R/nm	δ/nm	$2(R+\delta)$/nm
a	0.5	0.04	21	0.9	44	0.08	313	25	677
b	0.75	0.06	27	1.6	56	0.16	210	34	488
c	1.0	0.08	37	3.0	81	0.18	298	54	703

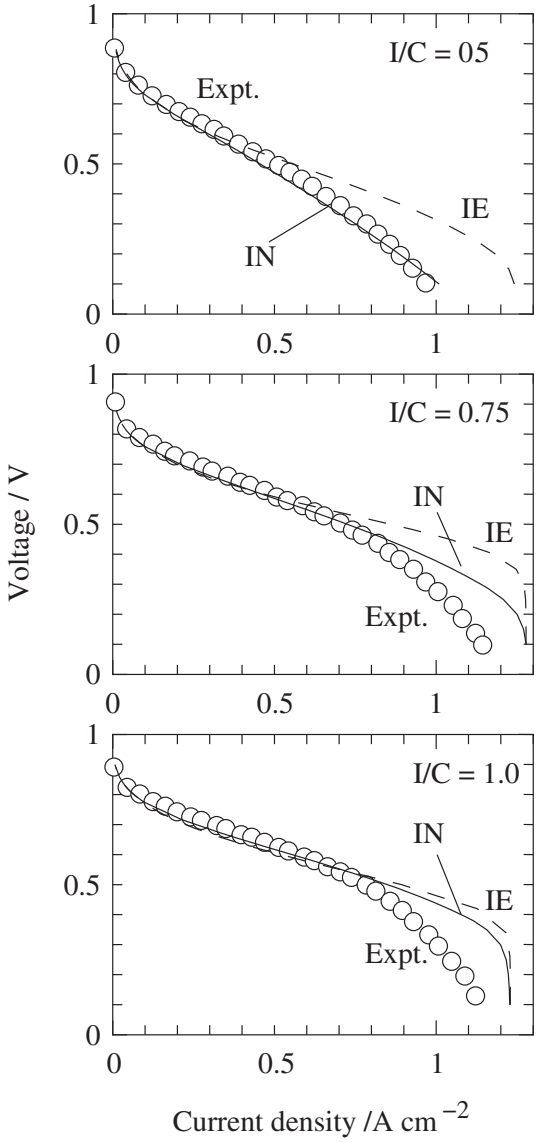

Fig. 10. Comparison of the predictions obtained using the IN (solid line) and IE (dashed line) models at an oxygen partial pressure of 9.3 kPa. Experimental results are represented by circles.

Fig. 10 shows predictions for current–voltage performance from the IN and IE models with the experimental data. Although the IN model gives a better fit to the experimental results than the IE model for I/C = 0.5, there is no significant difference between both fits. Therefore, both models can similarly predict the experimental results by the selection of an appropriate agglomerate size. Thus, the validity of the agglomerate model should be determined by how the model reflects the actual structure of the catalyst layer.

From this discussion, it is reasonable to attribute the hindrance of oxygen transport in the catalyst layer to slow oxygen dissolution at the gas–ionomer interface, rather than to large agglomerates. This implies that an increase in the gas–ionomer surface area and/or selection of an ionomer with a high oxygen dissolution rate are better strategies to enhance fuel cell performance than decreasing the agglomerate size.

5. Conclusions

A model of oxygen transport in the catalyst layer of PEFCs was developed. The model is based on the analysis of the oxygen transport properties of thin ionomer films cast on a Pt electrode on a quartz plate. The diffusion-limited current density of the *ORR* was measured as a function of film thickness. The current density could be explained by Fick's law of diffusion combined with the oxygen dissolution process from the gas phase to the ionomer. The rate of dissolution was determined as a term that is independent of film thickness. The dissolution rate is significant when the film is thinner than approximately 100 nm, from an order-of-magnitude estimate using the measured values of diffusivity and dissolution rate. The dissolution model was incorporated into the conventional agglomerate model with interface equilibrium and the results of these two models were compared. The size of the ionomer film-covered agglomerate was determined so that the model prediction of the diffusion-limited current density corresponded to the experimental value and was compared with SEM images of the FIB cross-sections of catalyst layers. The size for the developed IN model was close to that observed using SEM; however, that for the conventional IE model was much larger than the SEM observation. The model predictions for current–voltage performance were not significantly different. Therefore, it is reasonable to attribute the hindrance of oxygen transport in the catalyst layer to slow oxygen dissolution at the gas–ionomer interface, rather than to large agglomerates.

Acknowledgments

The authors would like to thank Juntaro Seki for SEM imaging and Yutaka Ohya for experimental support.

Appendix A. Material properties

The water content of the membrane and the ionomer in the anode catalyst layer is calculated according to the relationship for Nafion 117 [38]:

$$\lambda = 0.043 + 17.81a - 39.85a^2 + 36a^3 \tag{A.1}$$

However, the depression of water content in the cathode catalyst layer is assumed and approximated by:

$$\lambda = \frac{1}{2}\left(0.043 + 17.81a - 39.85a^2 + 36a^3\right). \tag{A.2}$$

The diffusion coefficient of water in the ionomer, D_{H_2O}, is calculated from the self-diffusion coefficient, D_{NMR}, using [1,40]:

$$D_{H_2O} = D_{NMR}\frac{\partial \ln a}{\partial \ln \lambda}\exp\left[2416\left(\frac{1}{303} - \frac{1}{T}\right)\right] \tag{A.3}$$

The value of D_{NMR} is derived from interpolation of the experimental data as a function of λ [41].

The electroosmotic coefficient of the ionomer, β, is unity for $\lambda \geq 1.4$ [42] and assumed to be zero at $\lambda = 0$. The interpolation is smooth at $0 < \lambda < 1.4$.

The proton conductivity of the ionomer, κ, is calculated according to [1]

$$\kappa = (0.5139\lambda - 0.326)\exp\left[1268\left(\frac{1}{303} - \frac{1}{T}\right)\right], \quad \lambda \geq 1 \tag{A.4}$$

for the membrane. The value at $\lambda = 1$ is used for $\lambda < 1$. For the catalyst layers, an approximation of the internal data for a film cast from DE2020 Nafion dispersion solution at 80 °C,

$$\kappa = \begin{cases} 2.0718\lambda - 4.7911, & \lambda \geq 2.5 \\ 2.0718 \times 2.5 - 4.7911, & 0 < \lambda < 2.5 \end{cases}, \tag{A.5}$$

is applied instead of Eq. (A.4).

Henry's law constant for hydrogen in the ionomer, K_{H_2}, is calculated according to [43]:

$$K_{H_2} = 0.101325 \times 0.255 \times 10^5 \exp(170/T). \tag{A.6}$$

Henry's law constant for oxygen in the ionomer, K_{O_2}, is calculated as: k_o

$$K_{O_2} = \frac{101325}{4.408 - 0.09712\lambda}, \tag{A.7}$$

based on the data for a 96 μm thick film cast from DE2020.

The diffusivity of oxygen is calculated from the data fit for the 96 μm thick cast film:

$$D_{O_2} = 1.14698 \times 10^{-10}\lambda^{0.708}. \tag{A.8}$$

The effective value of the diffusion coefficient and the proton conductivity are described by Bruggeman's approximation [32]. That is, the binary diffusion coefficient of the gas species in a porous component is given as:

$$\hat{D}_{ij}^{eff} = \varepsilon_0^{1.5}\hat{D}_{ij}. \tag{A.9}$$

The diffusion coefficient of water in the ionomer of the catalyst layer is given as:

$$D_{H_2O}^{eff} = \varepsilon_l^{1.5}D_{H_2O}. \tag{A.10}$$

The diffusion coefficient of oxygen in the agglomerate is given as:

$$D_{O_2}^{eff} = \varepsilon_{l,agg}^{1.5}D_{O_2}. \tag{A.11}$$

Nomenclature

a	water activity
C	gas concentration, mol m^{-3}
c	concentration in ionomer, mol m^{-3}
D	diffusion coefficient in ionomer, m^2 s^{-1}
$\hat{D}$	diffusion coefficient of gas species, m^2 s^{-1}
F	Faraday's constant, C mol^{-1}
i	current density, A m^{-2}
J	diffusive flux, mol m^{-2} s^{-1}
K	Henry's law constant, Pa mol^{-1} m^{-3}
k	rate constant, m s^{-1}
L	thickness, m
M	number of gas species
m	equivalent weight, kg eq^{-1}
N	flux, mol m^{-2} s^{-1}
n	number density of agglomerate, m^{-3}
n_α	number of electrons transferred per molecule in reaction α
p_{sat}	saturation water vapor pressure, Pa
R	agglomerate radius, m
R_u	universal gas constant, J mol^{-1} K^{-1}
r	radial distance from the center of an agglomerate, m
s	surface area per volume, m^{-1}
T	temperature, K
v	average gas velocity, m s^{-1}
X	mole fraction
x	through-plane position in an MEA, m
y	I/C

Greek

α	apparent transfer coefficient
β	number of water molecules accompanied by a proton
δ	thickness of ionomer film over agglomerate, m
ε	volume fraction
η	overpotential, V
κ	proton conductivity, S m^{-1}
λ	water content of ionomer
ρ_i	density of species *i*, kg m^{-3}
σ	catalyst loading, kg m^{-2}
Φ	volumetric rate of production, mol m^3 s^{-1}
ϕ	electrolyte potential, V

Superscripts

eff	effective
eq	equilibrium
R	at agglomerate–ionomer film interface
$R+\delta$	at the interface between gas and ionomer film that covers an agglomerate
ref	reference
s	surface

Subscripts

0	pore
1	one agglomerate
agg	agglomerate
CB	carbon black
CL	catalyst layer
f	film
H_2	hydrogen
H_2O	water
HOR	hydrogen oxidation reaction
I	ionomer
O_2	oxygen
ORR	oxygen reduction reaction
Pt	platinum
v	ionomer–gas interface

References

[1] T.E. Springer, T.A. Zawodzinski, S. Gottesfeld, J. Electrochem. Soc. 138 (1991) 2334.
[2] D. Bevers, M. Wöhr, K. Yasuda, K. Oguro, J. Appl. Electrochem. 27 (1997) 1254.
[3] K. Broka, P. Ekdunge, J. Appl. Electrochem. 27 (1997) 281.
[4] F. Jaouen, G. Lindbergh, G. Sundholm, J. Electrochem. Soc. 149 (2002) A437.
[5] J. Ihomen, F. Jaouen, G. Lindbergh, A. Lundblad, G. Sundholm, J. Electrochem. Soc. 149 (2002) A448.
[6] L. Pisani, M. Valentini, G. Murgia, J. Electrochem. Soc. 150 (2003) A1549.
[7] N.P. Siegel, M.W. Ellis, D.J. Nelson, M.R. von Spakovsky, J. Power Sources 128 (2004) 173.
[8] Q. Guo, V.A. Sethuraman, R.E. White, J. Electrochem. Soc. 151 (2004) A983.
[9] Q. Guo, R.E. White, J. Electrochem. Soc. 151 (2004) E133.
[10] D. Song, Q. Wang, Z. Liu, T. Navessin, S. Holdcroft, Electrochim. Acta 50 (2004) 731.
[11] K.-M. Yin, J. Electrochem. Soc. 152 (2005) A583.
[12] W. Sun, B.A. Peppley, K. Karan, Electrochim. Acta 50 (2005) 3359.
[13] R. Madhusudana Rao, R. Rengaswamy, J. Power Sources 158 (2006) 110.
[14] A.A. Shah, G.-S. Kim, W. Gervais, A. Young, K. Promislow, J. Li, S. Ye, J. Power Sources 160 (2006) 1251.
[15] L. Matamoros, D. Brüggemann, J. Power Sources 161 (2006) 203.
[16] S.-M. Chang, H.-S. Chu, J. Power Sources 161 (2006) 1161.
[17] C.Y. Du, T. Yang, P.F. Shi, G.P. Yin, X.Q. Cheng, Electrochim. Acta 51 (2006) 4934.
[18] K. Karan, Electrochem. Comm. 9 (2007) 747.
[19] A.A. Shah, G.-S. Kim, P.C. Sui, D. Harvey, J. Power Sources 163 (2007) 793.
[20] L. Matamoros, D. Brüggemann, J. Power Sources 172 (2007) 253.
[21] S.-M. Chang, H.-S. Chu, J. Power Sources 172 (2007) 790.
[22] D. Gerteisen, A. Hakenjos, J.O. Schumacher, J. Power Sources 173 (2007) 346.
[23] R. Madhusdana Rao, D. Bhattacharyya, R. Rengaswamy, S.R. Choudhury, J. Power Sources 173 (2007) 375.
[24] M. Secanell, K. Karan, A. Suleman, N. Djilali, Electrochim. Acta 52 (2007) 6318.
[25] D. Harvey, J.G. Pharoah, K. Karan, J. Power Sources 179 (2008) 209.
[26] S. Kamarajugadda, S. Mazumder, J. Power Sources 183 (2008) 629.
[27] D. Gerteisen, T. Heilmann, C. Ziegler, J. Power Sources 187 (2009) 165.
[28] A.J. Bard, L.R. Faulkner, Electrochemical Methods: Fundamental and Applications, second ed., John Wiley & Sons, Inc., 2001.
[29] A. Parthasarathy, C.R. Martin, S. Srinivasan, J. Electrochem. Soc. 138 (1991) 916.
[30] M.A. Islam, H. Buschatz, D. Paul, J. Memb. Sci. 204 (2002) 379.
[31] Y. Liu, C. Ji, W. Gu, J. Jorne, H.A. Gasteiger, J. Electrochem. Soc. 158 (2011) B614.
[32] R.E. De La Rue, C.W. Tobias, J. Electrochem. Soc. 106 (1959) 827.
[33] H. Jinnai, R.J. Spontak, T. Nishi, Mocromolecules 43 (2010) 1675.
[34] K. Shinozaki, H. Yamada, Y. Morimoto, J. Electrochem. Soc. 158 (2011) B467.
[35] V.A. Sethuraman, S. Khan, J.S. Jur, A.T. Haug, J.W. Weidner, Electrochim. Acta 54 (2009) 6850.
[36] A. Parthasarathy, S. Srinivasan, J.A. Appleby, C.R. Martin, J. Electrochem. Soc. 139 (1992) 2530.
[37] Y. Takamura, E. Nakashima, H. Yamada, A. Tasaka, M. Inaba, ECS Trans. 16 (2008) 881.
[38] Z. Siroma, R. Kakitsubo, N. Fujiwara, T. Ioroi, S. Yamazaki, K. Yasuda, J. Power Sources 189 (2009) 994.
[39] H.F.M. Mohamed, K. Ito, Y. Kobayashi, N. Takimoto, Y. Takeoka, A. Ohira, Polymer 49 (2008) 3091.
[40] S. Motupally, A.J. Becker, J.W. Weidner, J. Electrochem. Soc. 147 (2000) 3171.
[41] T.A. Zawodzinski, M. Neeman, L.O. Sillerud, S. Gotetsfeld, J. Phys. Chem. 95 (1991) 6040.
[42] T.A. Zawodzinski, J. Davey, J. Valerio, S. Gottesfeld, Electrochim. Acta 40 (1995) 297.
[43] R.F. Mann, J.C. Amphlett, B.A. Peppley, C.P. Thurgood, J. Power Sources 161 (2006) 768.